frontiers in Materials

ORIGINAL RESEARCH
published: 23 November 2020
doi: 10.3389/fmats.2020.590143

Structural and Thermodynamic Properties of the High-Entropy Alloy AlCoCrFeNi Based on First-Principles Calculations

Juefei Wu[1†], *Zhen Yang*[1,2†], *Jiawei Xian*[1], *Xingyu Gao*[1]*, *Deye Lin*[1,3]* and *Haifeng Song*[1,3]*

[1]Laboratory of Computational Physics, Institute of Applied Physics and Computational Mathematics, Beijing, China, [2]Institute for Applied Physics, University of Science and Technology Beijing, Beijing, China, [3]CAEP Software Center for High Performance Numerical Simulation, Beijing, China

During the past two decades, the high-entropy alloy AlCoCrFeNi has attracted much attention due to its outstanding thermal and mechanical properties under ambient conditions. However, the exploration on the thermodynamic properties of this alloy under high temperatures and high pressures is relatively insufficient. Combining structural modeling with the similar atomic environment (SAE) method and first-principles simulations with the modified mean-field potential (MMFP) approach, we studied the lattice and magnetic structure as well as the thermodynamic properties of the body-centered-cubic AlCoCrFeNi, through supercell simulations. AlCoCrFeNi was found to display a strong local lattice distortion compared with typical 3*d* high-entropy alloys; the ferromagnetic structure stable at 0 K was predicted to transform to the paramagnetic structure at the Curie temperature T_C = 279.75 K, in good agreement with previous calculations; the calculated equilibrium volumes, bulk modulus, and shock Hugoniot all agree well with available experimental data and other theoretical values. These results demonstrate the validity and reliability of our methods used to study the dynamic properties of AlCoCrFeNi, providing a promising scheme for accessing the dynamic properties of sophisticated high-entropy alloys.

Keywords: high-entropy alloy, ab initio calculations, thermodynamic properties, AlCoCrNiFe, lattice and magnetic structure

OPEN ACCESS

Edited by:
Peter Liaw,
The University of Tennessee, Knoxville, United States

Reviewed by:
Jijun Zhao,
Dalian University of Technology, China
Yiping Lu,
Dalian University of Technology, China

***Correspondence:**
Xingyu Gao
gao_xingyu@iapcm.ac.cn
Deye Lin
lin_deye@iapcm.ac.cn
Haifeng Song
song_haifeng@iapcm.ac.cn

†*These authors have contributed equally to this work.*

Specialty section:
This article was submitted to Structural Materials, a section of the journal Frontiers in Materials

Received: *31 July 2020*
Accepted: *21 October 2020*
Published: *23 November 2020*

Citation:
Wu J, Yang Z, Xian J, Gao X, Lin D and Song H (2020) Structural and Thermodynamic Properties of the High-Entropy Alloy AlCoCrFeNi Based on First-Principles Calculations. Front. Mater. 7:590143. doi: 10.3389/fmats.2020.590143

INTRODUCTION

High-entropy alloys (HEAs) or multi-principle–element alloys represent a special group of solid solutions containing five or more elements, where the concentration He et al., 2018, Korchuganov, 2018, Li et al., 2018 of each element is between 5 and 35 at. % (Cantor et al., 2004; Yeh et al., 2004; Zhang et al., 2014). Because of tunable compositions and unique microstructures, HEAs possess superior mechanical properties such as high hardness, outstanding strength and excellent fracture toughness (Li et al., 2019; Miracle, 2019). Different from conventional alloys with only one or two principal components such as steels, HEAs pave a new way for the design of novel alloys. Thus, HEAs have promising potential for application in various industrial fields, and have attracted great attention during the past two decades.

Among all the HEAs studied so far, $Al_xCoCrFeN$ is one kind under intensive investigations, mostly because its properties can be fine-tuned by the concentration of the Al element (Miracle,

2019). The concentration of Al has strong effects on the phase structure of $Al_xCoCrFeNi$, which consequently influences the mechanical, electronic, and magnetic properties of this alloy (Tong et al., 2005; Santodonato et al., 2015; Santodonato et al., 2018). According to Wang et al. (2012), when $x < 0.5$, $Al_xCoCrFeNi$ possesses the face-centered cubic (fcc) structure; when $x > 0.9$, $Al_xCoCrFeNi$ has the body-centered cubic (bcc) structure (with a chemically ordered B2 or disordered A2 structure); when $0.5 < x < 0.9$, the crystal structure of $Al_xCoCrFeNi$ is a mixture of fcc and bcc (A2 or B2). These results indicate that the addition of the element Al tends to stabilize the bcc structure. With increasing concentration of Al, the hardness and strength of $Al_xCoCrFeNi$ increases accordingly (Zhang et al., 2012). It is worth noting that, CoCrFeNi (equivalently $Al_xCoCrFeNi$ with $x = 0$) is paramagnetic at ambient conditions, while $Al_2CoCrFeNi$ ($Al_xCoCrFeNi$ with $x = 2$) becomes paramagnetic at a higher Curie temperature of around 430 ± 3 K (Tian et al., 2013).

Though most experimental and theoretical reports on $Al_xCoCrFeNi$ have been focusing on its mechanic properties at quasi-static strain-rates under ambient conditions, its responses under strong shock compression have gradually attracted more attention from researchers. The mechanical properties of the fcc phase of $Al_xCoCrFeNi$ were investigated experimentally by Kumar et al. (2015), Li et al. (2017), Zhang et al. (2017), Gangireddy et al. (2018) and Meyers et al. (2018) using the split Hopkinson pressure bar. They found that these alloys show high resistance to adiabatic shear location, high strain rate sensitivity, and high strain hardening rate due to complex multiple hardening mechanisms (He et al. (2018), Korchuganov (2018), Li et al. (2018)). Recently, Jiang et al. (2016) found that the equal molar ratio AlCoCrFeNi HEA (with the bcc structure) exhibits high Hugoniot elastic limit (HEL). They measured the shock Hugoniot of AlCoCrFeNi using the normal plate impact technique, and the shock yield stress was estimated with the von Mises yield criterion (Meyer, 1994). However, this work only covers a fairly low pressure range of the shock equation of state (EOS), and the shock EOS at high pressures and high temperatures is still lacking.

The EOS of materials is indispensable to many scientific research and technological applications, such as those related to high-velocity impact, shock waves, explosions, and high-power lasers (Golosnoy et al., 1994). First-principle calculations have been found to predict accurately the EOS and thermodynamics properties of many metals at high temperatures and high pressures (Fortov et al., 1998; Song et al., 2007; Song and Liu, 2007; Liu et al., 2016; Söderlind and Young, 2018). As for first-principles calculations of HEAs, challenging obstacles originate from how to deal with three aspects (Tian, 2017; Ikeda et al., 2019): 1) the chemical disorder, 2) the magnetic disorder (Šebesta et al., 2019; Tian et al., 2019), and 3) the lattice vibrational contributions to the free energy. The quasi-harmonic approximation (QHA) models (Ma et al., 2015; Song et al., 2016) are applicable at low temperatures, while the computational cost and time are significant using frozen phonon method or first-principles molecular dynamics simulations (Körmann et al., 2017). Therefore, we need to seek other ways to calculate the free energy of HEAs that balance both the accuracy and the efficiency.

In this work, we combine structural modeling with the similar atomic environment (SAE) method (Tian et al., 2020) and first-principles calculations with the modified mean-field potential (MMFP) approach (Song and Liu, 2007) to predict the EOS and thermodynamic properties of the bcc AlCoCrFeNi HEA. We first use the SAE method to construct representative supercell structures to describe the chemical disorder of AlCoCrFeNi. Then both ferromagnetic and paramagnetic structures are characterized with randomly distributed magnetic elements in the SAE supercell, and the static EOS and ground-state structural properties are obtained by first-principles calculations with structural relaxations. The calculated equilibrium volume, bulk modulus, and Curie temperature are found to agree well with the experimental data in Tian et al. (2013) and Jiang et al. (2016). Next, within the MMFP approach, the static EOS is used to establish a mean-field potential (MFP), to estimate efficiently the lattice vibrational contributions to the Helmholtz free energy. Following the above steps, the thermal EOS is set up, and thermodynamic properties at high temperatures and high pressures are predicted for the bcc AlCoCrFeNi. Moreover, we calculated the shock Hugoniot, and our results are in good agreement with the experimental data in Jiang et al. (2016). This provides a persuasive verification for our modeling of the lattice structure with magnetism and the corresponding thermal EOS.

The rest of this article is arranged as follows. In Section II, the computational methods and details are introduced. In Section III, the ground-state properties of ferromagnetic and paramagnetic structures of $Al_xCoCrFeNi$ are investigated. In Section IV, the thermal EOS and thermodynamic properties $Al_xCoCrFeNi$ at high temperatures and high pressures are predicted. Concluding remarks are made in the last section.

METHODOLOGY

In this section, we introduce the computational methods for modeling solid-solution structures and magnetic structure, as well as for predicting the free energy.

Modeling Solid-Solution Structures

Since local lattice distortions can be strong in HEAs (Song et al., 2017), for the bcc AlCoCrFeNi, the supercell approach should be more appropriate than the conventional coherent potential approximation (CPA) (Gyorffy, 1972). Very recently, we proposed a supercell modeling approach for random alloys, that is, the similar atomic environment (SAE) method (Tian et al., 2020). The SAE method has been thoroughly cross-validated with the special quasi-random structure (SQS) method (Zunger et al., 1990) and applied to study the phase stability of AlCoCrFeNi (Guan et al., 2020). In the SAE method, the similarity function quantitatively describes the deviation of the current configuration from the corresponding fully disordered one in terms of clusters with different sizes. In

practice, it suffices to consider both diatomic clusters and triatomic clusters (Liu et al., 2005).

We start from a 3 × 3 × 5 bcc supercell containing 90 atoms for AlCoCrFeNi. To apply the SAE method, with appropriate weight w_n (n = 2, 3) and cutoff radius r_n^c (n = 2, 3), we minimize the following objective function with respect to the atomic configuration σ:

$$f(\sigma, r_2^c, r_3^c) = \sum_{d(A_2)<r_2^c} w_2(A_2) g(A_2, \sigma) + \sum_{d(A_3)<r_3^c} w_3(A_3) g(A_3, \sigma), \tag{2.1}$$

where $g(A_n, \sigma)$ and $g(A_3, \sigma)$ stand for the similarity function associated with the diatomic clusters A_2 and triatomic clusters A_3, respectively. And the corresponding diameter of the cluster is denoted by $d(A_2)$ or $d(A_3)$. For the bcc AlCoCrFeNi, $g(A_2, \sigma)$ and $g(A_3, \sigma)$ are minimized to 0.08 and 0.26 after 20,000 Monte Carlo samplings over the atomic configurational space. And the minimized objective function becomes acceptable compared with the structural modeling of AlCoCrFeNi HEA in Tian et al. (2020).

Modeling Magnetic Structure

To consider the temperature induced magnetic structural transition, we need to describe the ferromagnetic (FM) and paramagnetic (PM) states of the bcc AlCoCrFeNi. For the ferromagnetic state, we perform colinear calculations for the structural relaxation. The paramagnetic state above the Curie temperature is modeled with the disordered local moment (DLM) approximation (Gyorffy et al., 1985). That is, spin-up and spin-down atoms with equal atomic fraction for the same elements are treated as different atomic species distributed randomly in the SAE supercell. Theoretically, we could construct a larger SAE supercell with PM state containing nine components: (18Al) (9Cr↑9Cr↓) (9Fe↑9Fe↓) (9Co↑9Co↓) (9Ni↑9Ni↓). In practice, due to the random distribution of the magnetic moments, we can describe the magnetic disorder by randomly specifying spin-up and spin-down for the atomic sites of each magnetic element. Consequently, we have considered both the chemical and the magnetic disorder in a 90-atom SAE supercell. The validity of the DLM approximation will be demonstrated in Section 3.

First-Principles Computational Details

In the present ab initio calculations, we employed the Vienna Ab initio Simulation Package (VASP) (Kresse and Furthmüller, 1996a; Kresse and Furthmüller, 1996b) based on the density functional theory (Hohenberg and Kohn, 1964; Kohn and Sham, 1965). The exchange-correlation functional was treated by the generalized gradient approximation of Perdew, Burkey, and Ernzerhof (Perdew et al., 1996). The electron-ion interaction was described by the projector augmented wave (PAW) method (Blochl, 1994). The plane-wave cutoff energy is 600 eV. The Brillouin zone is sampled with the special ***k***-mesh generated by the Monkhorst-Pack scheme (Monkhorst and Pack, 1976) with a k-point spacing of 0.03 $Å^{-1}$. The convergence tolerance is 10^{-4} eV for total energy and 0.03 eV/Å for the maximum force on each atom.

Free Energy and Thermal EOS Model

The key for the prediction of EOS and thermodynamic properties is to calculate the Helmholtz free-energy as a function of volume (or pressure) and temperature. For a solid alloy at temperature T with volume per atom V, the Helmholtz free energy can often be expressed as follows:

$$F(V,T) = E_c(V) + F_{ion}(V,T) + F_{el}(V,T) - TS_{mix} - TS_{mag}, \tag{2.2}$$

where E_c is the ground-state energy when ions are fixed at their lattice sites, F_{ion} stands for the vibrational contribution to the free energy from the ions, F_{el} represents contribution from the thermal excitation of the electrons when the ions are fixed at their lattice sites. For the paramagnetic AlCoCrFeNi HEA, the two entropic terms are estimated with the mean-field approximation as in (Tian et al., 2013). As a result, the mixing entropy of ideal solid-solution is given by

$$S_{mix} = -k_B \sum_{i=1}^{5} c_i \ln c_i, \tag{2.3}$$

and the magnetic entropy the evaluated as

$$S_{mag} = -k_B \sum_{i=1}^{5} c_i \ln(1+\mu_i), \tag{2.4}$$

where k_B is Boltzmann's constant, and c_i and μ_i are the concentration and the magnetic moment of the i-th element, respectively.

The ground-state energy E_c is obtained by first-principles calculations. The electronic contribution is estimated as $F_{el} = U_{el} - TS_{el}$, where the excited energy U_{el} and the electronic entropy S_{el} are calculated as

$$U_{el}(V,T) = \int f \cdot \varepsilon n(\varepsilon, \mathrm{V}) d\varepsilon - \int^{\varepsilon_F} \varepsilon n(\varepsilon, V) d\varepsilon, \tag{2.5}$$

$$S_{el}(V,T) = -k_B \int n(\varepsilon, V)[f \ln f + (1-f) ln(1-f)] d\varepsilon. \tag{2.6}$$

f is the Fermi-Dirac distribution function, and $n(\varepsilon, V)$ stands for the electronic density of state as a function of V.

To obtain the vibrational contribution, we employ the MMFP approach (Song and Liu, 2007), which is a generalization of the mean-field potential (MFP) approach proposed in Wang (2000) and Wang et al. (2000) for thermodynamics. By introducing additional freedoms associated with lattice parameters in MFP calculations, the MMFP method can be applied to more complicated systems (Song et al., 2007; Tian et al., 2015). The vibrational free energy F_{ion} includes the contribution from the harmonic motion of ions, as well as the anharmonic contribution which becomes significant at high temperatures. Among all methods to deal with the anharmonic contribution, MFP is one of the most efficient and has great potential for the prediction of the thermodynamic properties of multicomponent alloys.

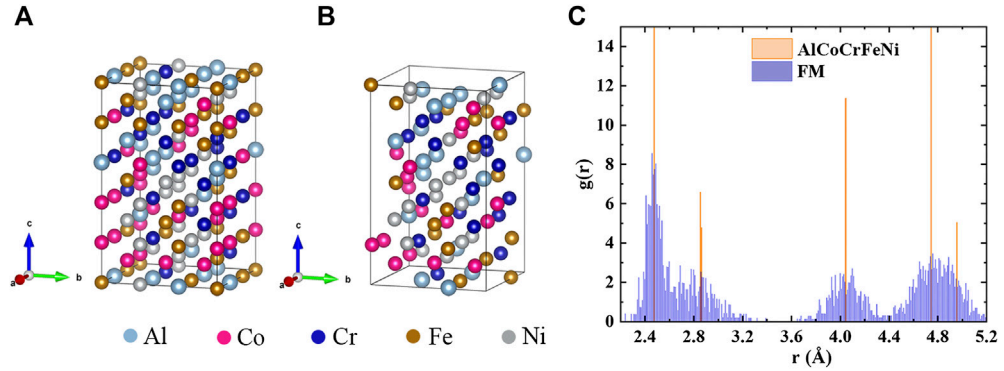

FIGURE 1 | The supercell structure of AlCoCrFeNi before (A) and (B) after optimization with FM, and (C) the corresponding radial distribution function. The spreading peaks illustrate lattice distortion after structure relaxation with FM.

LATTICE DISTORTION AND MAGNETIC STATES

According to Kao et al. (2009), the addition of Al destabilizes the fcc CoCrFeNi, and the associated local lattice distortion leads to the structural transformation to bcc when x ≥ 0.9 for Al in $Al_xCoCrFeNi$. Thus, local lattice distortion is an essential factor when studying HEAs (Song et al., 2017), and the supercell method is fully capable of evaluating it. We set the lattice parameters of the bcc (Wang et al., 2008; Wang et al., 2012) supercell according to experimental measurements (Kao et al., 2009). As shown in **Figure 1A**, the supercell contains 90 atoms with five elements randomly distributed.

We also performed an FM static calculation with the unrelaxed FM structure, to compare with that of the relaxed FM one (Tian et al., 2013). The total energy for unrelaxed FM structure is -6.81 eV/atom, while that for the relaxed FM structure is -6.85 eV/atom. This indicates that the relaxed FM structure is energetically more stable. The relaxed FM structure is displayed in **Figure 1B**, where distinct local distortions can be observed, quite different from the case for the unrelaxed FM structure in **Figure 1C**. To see how strong the lattice distortion is, we first compare the radial distribution functions (RDF) between the FM structure and the unrelaxed structure in **Figure 1C**. The unrelaxed structure has sharp peaks which represent interatomic distances from the first-nearest-neighboring (1NN) to the 5NN, while the peaks are broader in the relaxed FM structure, indicating the presence of the lattice distortion in the relaxed FM structure. Furthermore, we calculated the coefficient,

$$\Delta d = \frac{1}{N}\sum_i \sqrt{(x_i - x_i^{'})^2 + (y_i - y_i^{'})^2 + (z_i - z_i^{'})^2}, \qquad (3.1)$$

to evaluate local lattice distortions of the relaxed structure relative to the unrelaxed one quantitatively. Here, with respect to the lattice basis of unit cell, (x_i, y_i, z_i) and $(x_i^{'}, y_i^{'}, z_i^{'})$ are the reduced coordinates of the unrelaxed and relaxed positions of the FM structure, respectively. The calculated value $\Delta d = 0.05$ shows strong local lattice distortion than most 3d HEAs (Song et al., 2017). The calculated magnetic moments of the unrelaxed and relaxed FM structure are 0.78 μ_B/atom and 0.62 μ_B/atom, suggesting that lattice distortions can suppress the magnetic moments. As a result, it is necessary to consider the local lattice distortions of the AlCoCrFeNi HEA in line with previous theoretical calculations (Song et al., 2017).

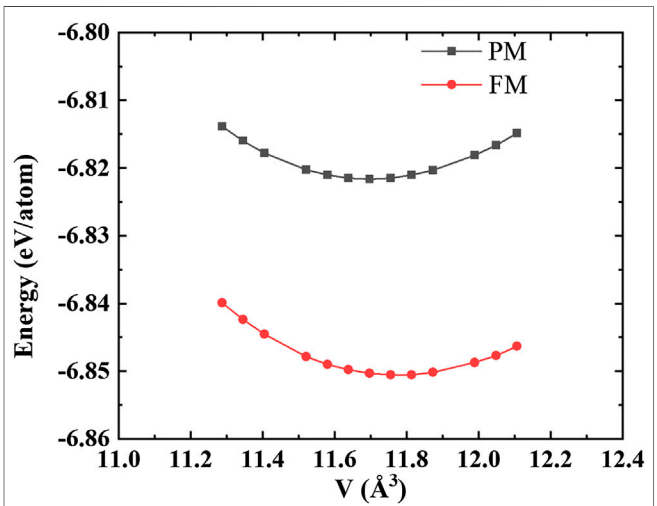

FIGURE 2 | E-V relation for PM structure and FM structure.

To investigate the properties of AlCoCrFeNi under ambient conditions (Tian et al., 2013), we propose to describe the paramagnetic state based on the relaxed FM structure. First, according to the above analysis, we found that ion positions have larger effect on the total energy than the magnetic configuration. Thus, modeling the AlCoCrFeNi under FM relaxation is appropriate for PM studies. Second, we use an approximate model to describe the PM state by randomly specifying spin-up and spin-down in each element and restrict the total magnetic moment to be zero in the subsequent static calculation with collinear magnetism. The resulting total energy of the PM structure is -6.82 eV/atom, larger than the relaxed FM structure -6.85 eV/atom. This is in agreement with the trend that

TABLE 1 | The volume and bulk modulus at 300 K and 1 bar

	V_0 (Å^3)	B_0 (GPa)
MFP	11.96	134
Cheng et al. (2019)	11.92	150±2.5

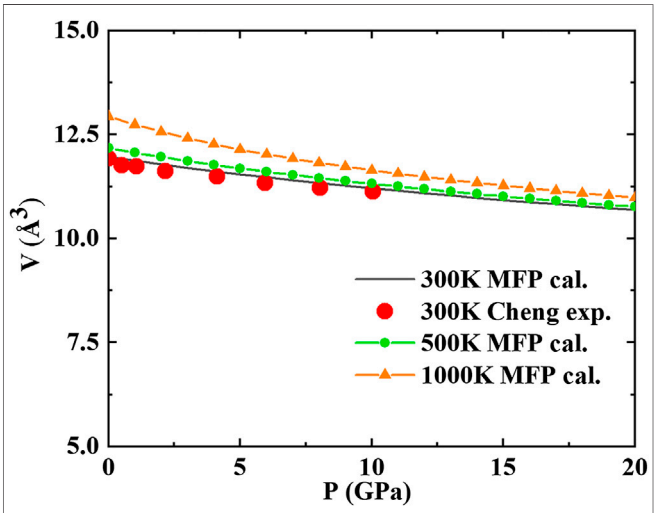

FIGURE 3 | $P - V_0/V$ relationship on Hugoniot. The solid line is calculated by MFP, and the dot symbols are experimental data from Jiang et al. (2016).

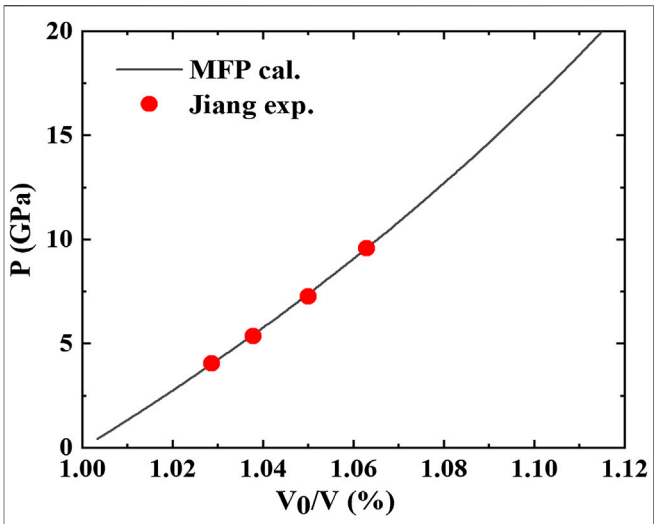

FIGURE 4 | $V - P$ relationship on isotherm from 300 to 1000 K calculated by MFP. The solid line, dot symbols line, triangle symbols line are $V - P$ relationship on 300, 500, 1000 K. The square symbols are from Cheng et al. (2019) XRD and DAC experiments result.

PM is the stable state under ambient conditions (Tian et al., 2013).

To further verify the model describing the PM state, we calculated the static E-V relation of the relaxed FM structure and PM structure under different volumes, and fit the E-V relation of the relaxed FM structure and PM structure, respectively, the results are shown in **Figure 2**. The ground-state volume of the PM structure is 11.67 Å^3/atom and the relaxed FM structure is 11.77 Å^3/atom, indicating that ferromagnetism leads to volume expansion. Moreover, the estimated ground-state energy for the PM structure is still larger than that of the relaxed FM structure. Besides, we calculated the Curie temperature T_C of AlCoCrFeNi within the mean-field approximation (Ge et al., 2018). In this approximation, T_C is expressed as follows:

$$T_c = \frac{2}{3(1-c)k_B}\left(E_{tot}^{PM} - E_{tot}^{FM}\right) = \frac{2}{3(1-c)k_B}\Delta E, \qquad (3.2)$$

where k_B is the Boltzmann's constant, $(E_{tot}^{PM} - E_{tot}^{FM})$ is the ground-state total energy difference between the PM and relaxed FM structure, and c is the concentration of nonmagnetic elements. Our estimated Curie temperature T_C = 279.75 K lies in the range of the critical temperature of Al_xCoCrFeNi estimated by Kao et al. (2011), which is between 200 K (x = 0.75) and 400 K (x = 1.25), demonstrating the validity of our model to describe PM structure. Therefore, the PM structure we have constructed is appropriate for the following thermodynamic calculations.

RESULTS FOR GROUND-STATE PROPERTIES

First of all, we have calculated the equilibrium volume and bulk modulus at room temperature as listed in Table 1. The difference is 0.04 Å^3/atom between the volume V_0 calculated by MFP and that given in the X-ray diffraction (XRD) experiment by Cheng et al. (2019). It seems that there is a relatively large difference between theory and experiment in the bulk modulus B_0. The bulk modulus provided by Cheng results from fitting the volume data from the Diamond anvil cell (DAC) experiments to the third-order Birch-Murnaghan EOS. The different ways to construct the EOS can influence the value of B_0 and lead to the large difference in B_0 observed here. Then we calculated the $V - P$ relationship at 300 K. In addition, we also computed the isotherm at 500 and 1000 K. We plot our results and Cheng's DAC data in **Figure 3**.

In **Figure 4**, we plot the thermal EOS of bcc AlCoCrFeNi at temperatures between 300 and 1000 K. The figure shows that our results at 300 K are in good agreement with experimental values. The calculated thermal EOS exactly goes through the equilibrium state derived from the experimental relation between the shock velocity and the particle velocity from Jiang et al. (2016). Since the relation between the shock velocity and the particle velocity depends largely on B_0, the good agreement with experiment sets up the confidence that our bulk modulus B_0 calculation is indeed reasonable. It is also shown in **Figure 4** that the total pressure for a given volume increases with increasing temperature due to the thermal pressure contribution from the electronic excitations and lattice vibrations.

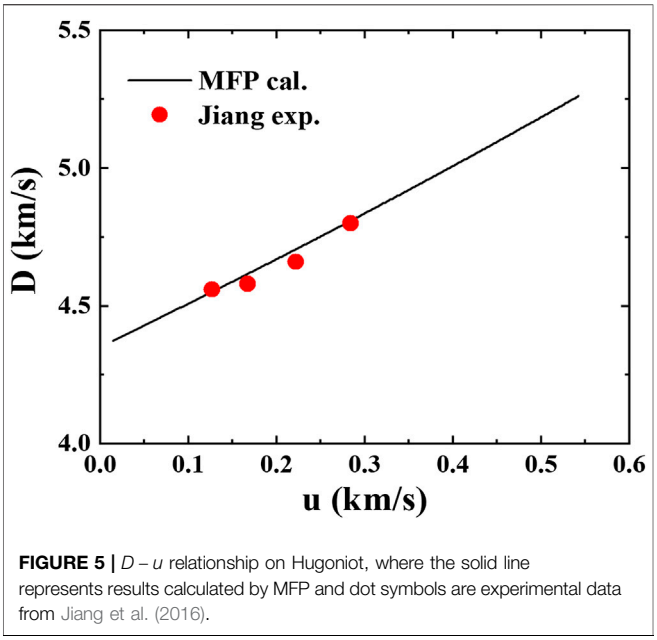

FIGURE 5 | $D-u$ relationship on Hugoniot, where the solid line represents results calculated by MFP and dot symbols are experimental data from Jiang et al. (2016).

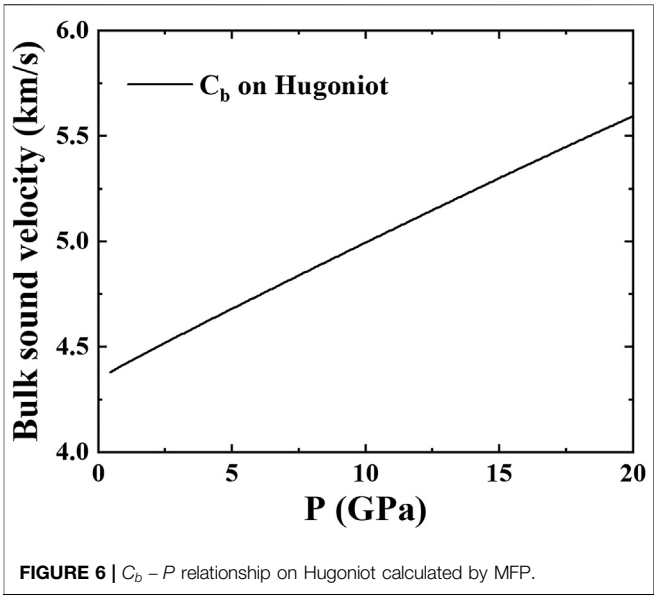

FIGURE 6 | $C_b - P$ relationship on Hugoniot calculated by MFP.

RESULTS FOR THERMODYNAMIC PROPERTIES

An important source of information on the EOS at high compressions and high temperatures is the shock wave data. Shock wave experiments often provides data for the shock velocity D and the particle velocity u. From the shock wave data, one can evaluate Hugoniot states as follows:

$$V_{\mathrm{H}} = V_0 \frac{D-u}{D}, \tag{4.1}$$

$$P_{\mathrm{H}} = \rho_0 D u, \tag{4.2}$$

where V_{H} and P_{H} stand for the volume and the pressure at the Hugoniot state, respectively, and V_0 and ρ_0 stand for the volume and density of the initial state at room temperature, respectively. To validate the calculated EOS of the bcc AlCoCrFeNi, we determine the Hugoniot states by solving the Rankine–Hugoniot equation:

$$U_{\mathrm{H}} - U_0 = \frac{1}{2}(P_0 + P_{\mathrm{H}})(V_0 - V_{\mathrm{H}}), \tag{4.3}$$

where U_{H} and U_0 represent the internal energy of the Hugoniot state and the initial state, respectively. The calculated Hugoniot states of the bcc AlCoCrFeNi are shown in **Figure 3**. The predicted $P - V_0/V$ relation below 10 GPa is in good agreement with the experimental data in Jiang et al. (2016).

Then the shock wave data can be derived from the calculated Hugoniot states as follows:

$$D = V_0 \left(\frac{P_{\mathrm{H}} - P_0}{V_0 - V_{\mathrm{H}}} \right)^{1/2}, \tag{4.4}$$

$$u = \left[(P_{\mathrm{H}} - P_0)(V_0 - V_{\mathrm{H}}) \right]^{1/2}, \tag{4.5}$$

which are plotted in **Figure 5**. The predicted $D - u$ relation below the particle velocity of 0.3 km/s is also in good agreement with the experimental data in Jiang et al. (2016). And the calculated shock wave data are extended to 0.55 km/s in the particle velocity. The good agreement provides a persuasive verification of the thermal EOS of the bcc AlCoCrFeNi. Based on the thermal EOS, we further obtain the bulk sound velocity C_b under shock compression. The results are shown in **Figure 6**.

Sound velocity is often measured in shock compression experiments. At present, there are not too much data for AlCoCrFeNi under shock compression. We calculate the bulk sound velocity C_b to give a reference for shock compression experiments design or verification.

CONCLUSION

In summary, three conclusions are made from our *ab initio* calculations.

(1) By constructing a supercell to study the local lattice distortion of AlCoCrFeNi, we found that the local lattice distortion has a strong effect on the structure of AlCoCrFeNi.
(2) On the basis of the relaxed ferromagnetic structure, we studied the paramagnetic state of AlCoCrFeNi, and showed that the Curie temperature is in line with previous estimated results and the E-V relation is in agreement with the experimental trend, suggesting the validity of the model to describe the paramagnetic structure.
(3) We calculate the equilibrium volumes, bulk modulus, and the shock Hugoniot equation of state of AlCoCrFeNi. Our results are in good agreement with the dynamic impact experiment. Our results show the validity and reliability of our methods to study the dynamic properties of AlCrFeCoNi, providing a promising scheme for investigating the thermodynamic properties of complicated high-entropy alloys.

DATA AVAILABILITY STATEMENT

All datasets presented in this study are included in the article/supplementary material.

AUTHOR CONTRIBUTIONS

JW and ZY have the same contribution to this work. All authors listed have made a substantial, direct and intellectual contribution to the work, and approved it for publication.

ACKNOWLEDGMENTS

We thank Fawei Zheng for the help with the calculations of paramagnetic structure. We thank Pro. Fuyang Tian for the help of supercell methods. We are grateful to Dr. Yu Liu and Dr. Dan Jian for calculations of elastic moduli and evaluation of lattice distortion. We acknowledge the support from the Science Challenge Project under Grant No. TZ2018002 and the National Key Research and Development Program of China under Grant No. 2016YFB0201204.

REFERENCES

Blochl, P. E. (1994). Projector augmented-wave method. *Phys. Rev. B* 50, 17953. doi:10.1103/physrevb.50.17953.

Cantor, B., Chang, I. T. H., Knight, P., and Vincent, A. J. B. (2004). Microstructural development in equiatomic multicomponent alloys. *Materials Science and Engineering: A.* 375–377 213–218. doi:10.1016/j.msea.2003.10.257.

Cheng, B., Zhang, F., Lou, H., Chen, X., Liaw, P. K., Yan, J., and Zeng, Q. (2019). Pressure-induced phase transition in the AlCoCrFeNi high-entropy alloy. *Scripta Materialia.*, 161, 88-92. doi:10.1016/j.scriptamat.2018.10.020.

Fortov, V. E., Khishchenko, K. V., Levashov, P. R., and Lomonosov, I. V. (1998). Nuclear instruments and methods in physics research section A: accelerators, spectrometers, detectors and associated equipment. *Phys. Res.* 415, 604–608. doi:10.1016/S0168-9002(98)00405-7.

Gangireddy, S., Gwalani, B., Liu, K., Banerjee, R., and Mishra, R. S. (2018). Microstructures with extraordinary dynamic work hardening and strain rate sensitivity in Al0.3CoCrFeNi high entropy alloy. *Materials Science and Engineering: A.* 734, 42–50. doi:10.1016/j.msea.2018.07.088.

Ge, H., Song, H., Shen, J., and Tian, F. (2018). Effect of alloying on the thermal-elastic properties of 3d high-entropy alloys, *Mater. Chem. Phys.* 210, 320-326. doi:10.1016/j.matchemphys.2017.10.046

Golosnoy, I. O., Kalitkin, N. N., and Volokitin, V. S. Wide-range equation of state of matter. I. Analysis of nonideality models, *Russ. Phys. J.* 37, 1029–1047 (1994).

Guan, H. Q., Huang, S. S., Ding, J. H., Tian, F. Y., Xu, Q., and Zhao, J. J. (2020). Chemical environment and magnetic moment effects on point defect formations in CoCrNi-based concentrated solid-solution alloys. *Acta Materialia.* 187, 122 doi:10.1016/j.actamat.2020.01.044.

Gyorffy, B. L. Coherent-potential approximation for a nonoverlapping-muffin-tin-potential model of random substitutional alloys. (1972). *Phys. Rev. B.* 5, 2382. doi:10.1103/PhysRevB.5.2382.

Gyorffy, B. L., Pindor, A. J., Staunton, J., Stocks, G. M., and Winter, H. (1985). A first-principles theory of ferromagnetic phase transitions in metals. *J. Phys. F Met. Phys.* 15, 1337. doi:10.1088/0305-4608/15/6/018.

He, J., Wang, Q., Zhang, H., Dai, L., Mukai, T., Wu, Y., et al. (2018). Dynamic deformation behavior of a face-centered cubic FeCoNiCrMn high-entropy alloy, *Sci. Bull.* 63 362–368. doi:10.1016/j.scib.2018.01.022.

Hohenberg, P., and Kohn, W. (1964). Inhomogeneous electron gas. *Phys. Rev.* 136(3B), B864. doi:10.1103/physrev.136.b864.

Ikeda, Y., Grabowski, B., and Körmann, F. (2019). Ab initio phase stabilities and mechanical properties of multicomponent alloys: a comprehensive review for high entropy alloys and compositionally complex alloys. *Mater. Char.* 147 464–511. doi:10.1016/j.matchar.2018.06.019.

Jiang, Z. J., He, J. Y., Wang, H. Y., Zhang, H. S., Lu, Z. P., and Dai, L. H. (2016). Shock compression response of high entropy alloys. *Mater. Res. Let.* 4, 226–232. doi:10.1080/21663831.2016.1191554.

Kao, Y. F., Chen, S. K., Chen, T. J., Chu, P. C., Yeh, J. W., and Lin, S. J. (2011). Electrical, magnetic, and Hall properties of $Al_xCoCrFeNi$ high-entropy alloys, *J. Alloys Compd.* 509, 1607–1614. doi:10.1016/j.jallcom.2010.10.210

Kao, Y.-F., Chen, T.-J., Chen, S.-K., and Yeh, J. -W. (2009). Microstructure and mechanical property of as-cast, -homogenized, and -deformed $Al_xCoCrFeNi$ ($0 \le x \le 2$) high-entropy alloys. *J. Alloys Compd.* 488, 57–64. doi:10.1016/j.jallcom.2009.08.090

Kohn, W., and Sham, L. J. Self-consistent equations including exchange and correlation effects. *Phys. Rev.* 140(4A), A1133 (1965). doi:10.1103/physrev.140.a1133.

Korchuganov, A. V. (2018). Onset of plastic deformation in non-equiatomic fcc CoCrFeMnNi high-entropy alloys under high-rate loading. *Letters on Materials.* 8, 311–316. doi:10.22226/2410-3535-2018-3-311-316.

Körmann, F., Ikeda, Y., Grabowski, B., and Sluiter, M. H. F. (2017). Phonon broadening in high entropy alloys. *Npj Computational Materials.* 3, 36. doi:10.1038/s41524-017-0037-8.

Kresse, G., and Furthmüller, J. (1996a). Efficiency iterative schemes for ab initio total-energy calculations using a plane-wave basis set. *Phys. Rev. B.* 54, 11169. doi:10.1103/PhysRevB.54.11169.

Kresse, G., and Furthmüller, J. (1996b). Efficiency of ab-initio total energy calculations for metals and semiconductors using a plane-wave basis set, *Computiontal Materials Science.* 6, 15. doi:10.1016/0927-0256(96)00008-0.

Kumar, N., Ying, Q., Nie, X., Mishra, R. S., Tang, Z., Liaw, P. K., et al. (2015). High strain-rate compressive deformation behavior of the Al0.1CrFeCoNi high entropy alloy. *Mater. Des.* 86, 598–602. doi:10.1016/j.matdes.2015.07.161.

Li, Z., Zhao, S., Alotaibi, S. M., Liu, Y., Wang, B., and Meyers, M. A. (2018). Adiabatic shear localization in the CrMnFeCoNi high-entropy alloy, *Acta Materialia.* 151, 424–431. doi:10.1016/j.actamat.2018.03.040.

Li, Z., Zhao, S., Diao, H., Liaw, P. K., and Meyers, M. A. (2017). High-velocity deformation of Al0.3CoCrFeNi high-entropy alloy: remarkable resistance to shear failure. *Sci. Rep.* 7, 42742. doi:10.1038/srep42742.

Li, Z., Zhao, S., Ritchie, R. O., and Meyers, M. A. (2019). Mechanical properties of high-entropy alloys with emphasis on face-centered cubic alloys. *Prog. Mater. Sci.* 102, 296–345. doi:10.1016/j.pmatsci.2018.12.003.

Liu, H., Song, H., Zhang, Q., Zhang, G., and Zhao, Y. (2016). Validation for equation of state in wide regime: copper as prototype, *Matter and Radiation at Extremes.* 1, 123–131. doi:10.1016/j.mre.2016.03.002.

Liu, J. Z., Van De Walle, A., Ghosh, G., and Asta, M. (2005). Structure, energetics, and mechanical stability of Fe-Cu bcc alloys from first-principles calculations. *Phys. Rev. B.* 72, 144109. doi:10.1103/PhysRevB.72.144109.

Ma, D., Grabowski, B., Körmann, F., Neugebauer, J., and Raabe, D. (2015). Ab initio thermodynamics of the CoCrFeMnNi high entropy alloy: importance of entropy contributions beyond the configurational one. *Acta Materialia.* 100 90–97. doi:10.1016/j.actamat.2015.08.050.

Meyer, M. A. *Dynamic behavior of materials.*, John Wiley & Sons, New York, (1994).

Meyers, M. A., Li, Z., Zhao, S., Wang, B., Liu, Y., and Liaw, P. K. (2018). Shear localization of fcc high-entropy alloys, *EPJ Web Conf.* 183, 03028. doi:10.1051/epjconf/201818303028.

Miracle, D. B. (2019). High entropy alloys as a bold step forward in alloy development. *Nat. Commun.* 10. doi:10.1038/s41467-019-09700-1.

Monkhorst, H. J., and Pack, J. D. (1976). Special points for Brillouin-zone integrations. *Phys. Rev. B.* 16, 1748. doi:10.1103/physrevb.13.5188.

Perdew, J. P., Burke, K., and Ernzerhof, M. (1996). Generalized gradient approximation made simple. *Phys. Rev. Lett.* 77, 3865. doi:10.1103/physrevlett.77.3865.

Santodonato, L. J., Liaw, P. K., Unocic, R. R., Bei, H., and Morris, J. R. (2018). Predictive multiphase evolution in Al-containing high-entropy alloys. *Nat. Commun.* 9, 4520. doi:10.1038/s41467-018-06757-2.

Santodonato, L. J., Zhang, Y., Feygenson, M., Parish, C. M., Gao, M. C., Weber, R. J. K., et al. (2015). Deviation from high-entropy configurations in the atomic

distributions of a multi-principal-element alloy, *Nat. Commun.* 6, 5964 doi:10.1038/ncomms6964.

Šebesta, J., Carva, K., and Legut, D. (2019). Role of magnetism in the stability of the high-entropy alloy CoCrFeMnNi and its derivatives. *Phys. Rev. Mater.* 3. doi:10.1103/PhysRevMaterials.3.124410.

Song, H.-F., and Liu, H.-F. (2007). Modified mean-field potential approach to thermodynamic properties of a low-symmetry crystal: beryllium as a prototype. *Phys. Rev. B.* 75. doi:10.1103/PhysRevB.75.245126.

Song, H.-F., Liu, H.-F., and Tian, E. (2007). Structural and thermodynamic properties of hexagonal BeO at high pressures and temperatures, *J. Phys. Condens. Matter.* 19 456209. doi:10.1088/0953-8984/19/45/456209.

Song, H., Tian, F., and Wang, D. (2016). Thermodynamic properties of refractory high entropy alloys, *J. Alloys Compd.* 682, 773–777. doi:10.1016/j.jallcom.2016.04.320.

Song, H. Q., Tian, F. Y., Hu, Q. M., Vitos, L., and Chen, N. X. (2017). Local lattice distortion in high-entropy alloys, *Phys Rev Mater.* 1, 023404. doi:10.1103/PhysRevMaterials.1.023404.

Söderlind, P., and Young, D. (2018). Assessing density-functional theory for equation-of-state. *Computation.* 6 13. doi:10.3390/computation6010013.

Tian, F. (2017). A review of solid-solution models of high-entropy alloys based on ab initio calculations. *Frontiers in Materials.* 4. doi:10.3389/fmats.2017.00036.

Tian, F., Delczeg, L., Chen, N., Varga, L. K., and Vitos, L. (2013). Structural stability of $NiCoFeCrAl_x$ high-entropy alloy from ab initio theory. *Phys. Rev. B.* 88, 085128. doi:10.1103/PhysRevB.88.085128.

Tian, F., Zhao, H., Wang, Y., and Chen, N. (2019). Investigating effect of ordering on magnetic-elastic property of FeNiCoCr medium-entropy alloy. *Scripta Materialia.* 166, 164–167. doi:10.1016/j.scriptamat.2019.03.023.

Tian, F. Y., Lin, D.-Y., Gao, X. Y., Zhao, Y.-F., and Song, H.-F. (2020). A structural modeling approach to solid solutions based on the similar atomic environment. *J. Chem. Phys.* 153, 034101. doi:10.1063/5.0014094.

Tian, M. F., Song, H. F., Liu, H. F., Wang, C., Fang, Z., and Dai, X. (2015). Thermodynamics of the α -γ transition in cerium studied by an LDA + Gutzwiller method. *Phys. Rev. B.* 91, 125148. doi:10.1103/PhysRevB.91.125148.

Tong, C.-J., Chen, Y.-L., Yeh, J.-W., Lin, S.-J., Chen, S.-K., Shun, T.-T., et al. (2005). Microstructure characterization of AlxCoCrCuFeNi high-entropy alloy system with multiprincipal elements. *Metall. Mater. Trans.* 36, 881–893. doi:10.1007/s11661-005-0283-0.

Wang, W.-R., Wang, W.-L., Wang, S.-C., Tsai, Y.-C., Lai, C.-H., and Yeh, J.-W. (2012). Effects of Al addition on the microstructure and mechanical property of $Al_xCoCrFeNi$ high-entropy alloys. *Intermetallics.* 26, 44-51. doi:10.1016/j.intermet.2012.03.005

Wang, Y. (2000). Classical mean-field approach for thermodynamics: ab initio thermophysical properties of cerium. *Phys. Rev. B.* 61, R11863. doi:10.1103/PhysRevB.61.R11863.

Wang, Y., Chen, D., and Zhang, X. (2000). Calculated equation of state of Al, Cu, Ta, Mo, and W to 1000 GPa, *Phys. Rev. Lett.* 84, 3220. doi:10.1103/PhysRevLett.84.3220.

Wang, Y.-P., Li, B.-S., Ren, M.-X., Yang, C., and Fu, H.-Z. (2008). Microstructure and compressive properties of AlCrFeCoNi high entropy alloy, *Mater. Sci. Eng.* 491 154–158. doi:10.1016/j.msea.2008.01.064

Yeh, J.-W., Chen, S.-K., Lin, S.-J., Gan, J.-Y., Chin, T.-S., Shun, T.-T., et al. (2004). Nanostructured high-entropy alloys with multiple principal elements: novel alloy design concepts and outcomes, *Adv. Eng. Mater.* 6, 299–303. doi:10.1002/adem.200300567.

Zhang, C., Zhang, F., Chen, S., and Cao, W. (2012). Computational thermodynamics aided high-entropy alloy design. *JOM.* 64, 839–845. doi:10.1007/s11837-012-0365-6.

Zhang, T. W., Jiao, Z. M., Wang, Z. H., and Qiao, J. W., (2017). Dynamic deformation behaviors and constitutive relations of an AlCoCr1.5Fe1.5NiTi0.5 high-entropy alloy. *Scripta Materialia.* 136, 15–19. doi:10.1016/j.scriptamat.2017.03.039.

Zhang, Y., Zuo, T. T., Tang, Z., Gao, M. C., Dahmen, K. A., Liaw, P. K., et al. (2014). Microstructures and properties of high-entropy alloys. *Prog. Mater. Sci.* 61, 1–93. doi:10.1016/j.pmatsci.2013.10.001.

Zunger, A., Wei, S. H., Ferreira, L. G., and Bernard, J. E. (1990). Special quasirandom structures. *Phys. Rev. Lett.* 65, 353. doi:10.1103/PhysRevLett.65.353.

Conflict of Interest: The authors declare that the research was conducted in the absence of any commercial or financial relationships that could be construed as a potential conflict of interest.